Research Article Vol. 8, No. 12 / December 2021 / Optica 1515

Deterministic photonic quantum computation in a synthetic time dimension

Ben Bartlett,[1,2,3] Avik Dutt,[2] and Shanhui Fan[2,*]

[1]Department of Applied Physics, Stanford University, Stanford, California 94305, USA
[2]Department of Electrical Engineering, Stanford University, Stanford, California 94305, USA
[3]e-mail: benbartlett@stanford.edu
*Corresponding author: shanhui@stanford.edu

Received 8 March 2021; revised 20 July 2021; accepted 21 October 2021 (Doc. ID 424258); published 29 November 2021

Photonics offers unique advantages as a substrate for quantum information processing, but imposes fundamental scalability challenges. Nondeterministic schemes impose massive resource overheads, while deterministic schemes require prohibitively many identical quantum emitters to realize sizeable quantum circuits. Here we propose a scalable architecture for a photonic quantum computer that needs minimal quantum resources to implement any quantum circuit: a single coherently controlled atom. Optical switches endow a photonic quantum state with a synthetic time dimension by modulating photon–atom couplings. Quantum operations applied to the atomic qubit can be teleported onto photonic qubits via projective measurement, and arbitrary quantum circuits can be compiled into a sequence of these teleported operators. This design negates the need for many identical quantum emitters to be integrated into a photonic circuit and allows effective all-to-all connectivity between photonic qubits. The proposed device has a machine size that is independent of quantum circuit depth, does not require single-photon detectors, operates deterministically, and is robust to experimental imperfections.

https://doi.org/10.1364/OPTICA.424258

1. INTRODUCTION

Photonics offers many advantages for quantum information processing [1–3]: optical qubits have very long coherence times, are maintainable at room temperature, and are optimal for quantum communication. The main difficulty faced by all quantum computing (QC) architectures is scalability, but this is especially true for photonic systems. Optical qubits must propagate, so processing must be done mid-flight by passing the photons through sequential optical components. Since photonic quantum gates are physical objects (as opposed to, e.g., sequential laser pulses for atomic qubits), machine size scales with circuit depth, making complex quantum circuits prohibitively large to implement even using compact integrated photonics.

Further limiting the scalability of photonic quantum computers is the difficulty of integrating many high-fidelity multi-photon gates into an optical circuit. This is an issue for both nondeterministic gate schemes [4,5], which impose massive resource overheads for fault tolerant operation due to low gate success probabilities [6], and deterministic scattering-based approaches [7–11]. Although scattering-based two-photon gates can be individually implemented with high fidelity [12–16], unrealistically large numbers of identical quantum emitters are needed to realize sizeable quantum circuits [17], a problem exacerbated in solid-state quantum emitters by poor indistinguishability due to homogeneous and inhomogeneous broadening [18,19]. An architecture for a quantum computer that uses only a single quantum emitter to implement all gates in a quantum circuit would thus substantially improve the scalability and experimental feasibility of scattering-based photonic quantum computation.

Here we show that the emerging concept of synthetic dimensions [20,21] naturally lends itself to such an architecture. Synthetic dimensions have recently generated great interest for exploring topological physics in photonics [22], but have not been extensively applied to quantum photonic systems. To form a synthetic dimension, one designs the couplings between states of a system, by either repurposing the usual geometric dimensions, such as space [23] or time [24–30], or augmenting these dimensions with internal degrees of freedom, such as frequency [31–36], spin [37–40], orbital angular momentum [41,42], or Floquet-induced side bands [43,44]. Since couplings between states within the synthetic dimension can be dynamically reconfigured and are not fixed by physical structure, one can scalably implement lattices with intricate connectivity. This allows multiple photonic qubits to be manipulated in synthetic space by a single quantum emitter without requiring spatially separated structures.

Our proposed design consists of a fiber loop coupled to a cavity containing a single coherently controlled atomic qubit. Optical switches endow counter-circulating photonic states with a synthetic temporal dimension by allowing coupling between these states. By scattering photons against the atom and subsequently rotating and projectively measuring the atomic state, operations can be teleported onto the photonic qubits; these operations can be composed to deterministically construct any quantum circuit. Readout of the photonic quantum state can be performed without

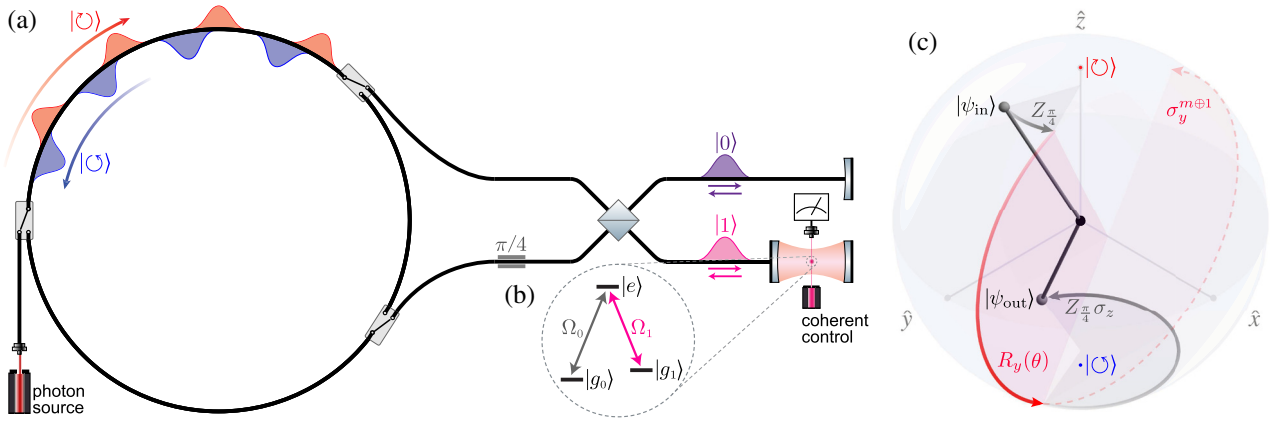

Fig. 1. Photonic quantum computer architecture described in this work. (a) Physical design of the device. Photonic qubits counterpropagate through a fiber storage ring, and optical switches can selectively direct photons through a scattering unit to interact with an atom in a cavity that is coherently controlled by a laser. (b) Energy structure of the atom: Ω_1 is resonant with the cavity mode and photon carrier frequency, while Ω_0 is far-detuned. (c) Bloch sphere depiction of the state of a photonic qubit in the $\{|\circlearrowleft\rangle, |\circlearrowright\rangle\}$ basis and an operation applied by one pass through the scattering unit. The rotations about $\hat{z}$ by fixed angles (gray) are applied by the phase shifter and beam splitter, while the rotation about $\hat{y}$ by a controllable angle θ (solid red) is applied to the atom using the cavity laser. Projectively measuring the atom teleports this rotation onto the photon, but may overshoot the target angle θ by π (dotted red) depending on the measurement outcome m. This operation is a universal single-qubit primitive: by composing several of these operations and adapting subsequent rotation angles based on measurement outcomes, arbitrary single-qubit gates can be deterministically constructed. See Visualization 1.

the need for single-photon detectors by sequentially swapping the state of the atom with each photonic qubit.

Our scheme has several unique characteristics. Most notably, the only controllable quantum resource is the single atomic qubit, which serves as a proxy to indirectly manipulate the photonic qubits. All quantum [45] operations and measurements on the photonic qubits are carried out by operations performed on this atom that are teleported onto the photons. This reduces the primary implementation challenge to preparing a single strongly coupled atom–cavity system, which has been experimentally demonstrated many times [10,16,46–51]. The synthetic time dimension allows the single atom to serve as the nonlinearity for all quantum gates and provides effective all-to-all connectivity between photonic qubits. The programmable nature of the teleported gates allows the atom to sequentially apply each required single- and two-photon gate without complex photon routing. This negates the requirement of conventional photonic QC schemes for many identical quantum emitters to be integrated into a photonic circuit. Finally, this design does not require single-photon detectors, which are a significant limitation to photonic QC. Instead, measurement of the atomic state can be performed with near-100% efficiency using the quantum jump technique, greatly improving the scalability of this design [9,47,52].

2. DESIGN

The architecture for the scheme is shown in Fig. 1(a). Qubits are encoded as trains of single-photon pulses counterpropagating through an optical storage ring, where the two propagation directions $\{|\circlearrowleft\rangle, |\circlearrowright\rangle\}$ form the computational basis. A single-photon source injects photon pulses into the ring; each photon is spectrally narrow about a carrier frequency ω_c, has a pulse width τ, and occupies its own time bin with temporal spacing $\Delta t \gg \tau$. (The photon source need not be deterministic as long as the time bin of each photon can be resolved. Alternately, a dedicated single-photon source may not be needed, as the atom–cavity system discussed below could itself be used as the source by using the control laser to excite the atom [53,54].)

The storage ring contains a pair of asymmetrically placed [55] optical switches that can selectively direct photons from the ring through a static 50:50 beam splitter and $\pi/4$ phase shifter and into a pair of waveguides. One of these waveguides is coupled to a cavity containing a single atom with a Λ-shaped three-level energy structure, shown in Fig. 1(b). The atom has nondegenerate ground states $|g_0\rangle$ and $|g_1\rangle$ and an excited state $|e\rangle$, and the $|g_1\rangle \leftrightarrow |e\rangle$ transition at frequency Ω_1 is resonant with cavity mode frequency and photon carrier frequency ω_c. The atom is coherently controlled by a laser that applies rotations between $|g_0\rangle$ and $|g_1\rangle$, and its state can be measured in the $\{|g_0\rangle, |g_1\rangle\}$ basis. We refer to the subsystem consisting of everything except the storage ring and photon source [the right half of Fig. 1(a)] as the "scattering unit." The round-trip optical path length through the scattering unit is matched to the path length around the storage ring so that a photon returns to its original time bin after passing through the scattering unit.

After a photon scatters against the atom and is returned to the storage ring, a rotation is applied to the state of the atomic qubit and a projective measurement is performed, teleporting the rotation onto the photonic qubit, as shown in the next section. By composing three of these teleported rotations, arbitrary single-qubit gates can be deterministically constructed. A controlled phase-flip ($c\sigma_z$) gate between two photons can also be constructed with a similar process, enabling universal quantum computation. Readout of the final quantum state can be performed without the need for single-photon detectors by sequentially swapping the state of the atom with each photonic qubit.

A. Rotation Teleportation Mechanism

Here we outline the mechanism by which a rotation gate may be teleported onto a photonic qubit; we show in the next section that by composing these teleported rotations, arbitrary single-qubit gates may be constructed. A derivation of the mechanism

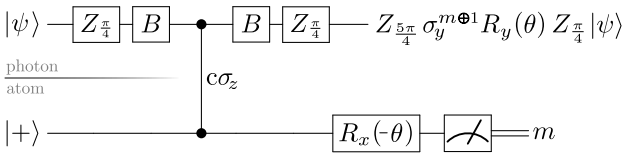

Fig. 2. Quantum gate sequence corresponding to one pass of a photon through the scattering unit. The projective measurement teleports the rotation applied to the atomic qubit onto the photonic qubit.

described here is shown in greater detail in Supplement 1 [56]. Suppose we wish to apply a rotation to photon j, which occupies time bin t_j and is circulating in the storage ring in state $|\Psi_{\text{in}}\rangle = \alpha|\circlearrowleft\rangle + \beta|\circlearrowright\rangle$, where $|\circlearrowleft\rangle$ and $|\circlearrowright\rangle$ denote the two counter-circulating states. While the optical switches are in the "closed" state, photons remain inside the storage ring; to operate on photon j, we "open" the switches at time $t_j - \Delta t/2$ and close them again at $t_j + \Delta t/2$ to direct photon j into the scattering unit. The photon passes through a $\pi/4$ phase shifter, which applies (up to a global phase) a $Z_{\frac{\pi}{4}} \equiv R_z(\pi/4) = \begin{pmatrix} e^{-i\pi/8} & 0 \\ 0 & e^{i\pi/8} \end{pmatrix}$ rotation, and a 50:50 beam splitter, which applies $B = \frac{1}{\sqrt{2}}\begin{pmatrix} 1 & i \\ i & 1 \end{pmatrix}$. Before interacting with the atom, the photon is a superposition of modes in the top and bottom waveguides; we label these spatial modes as $|0\rangle$ and $|1\rangle$, respectively. We can thus relate the basis states of the ring and scattering unit via the unitary transformation $\{|0\rangle, |1\rangle\} = BZ_{\frac{\pi}{4}}\{|\circlearrowleft\rangle, |\circlearrowright\rangle\}$.

The $|0\rangle$ component of the photon state is reflected by a mirror in the top waveguide, imparting a π phase shift, while the $|1\rangle$ component undergoes a cavity-assisted interaction with the atom in the bottom waveguide, which is initialized in the state $|+\rangle \equiv \frac{1}{\sqrt{2}}(|g_0\rangle + |g_1\rangle)$. The $|g_1\rangle \leftrightarrow |e\rangle$ transition frequency Ω_1 is resonant with the cavity mode and photon frequency ω_c, while the $|g_0\rangle \leftrightarrow |e\rangle$ frequency Ω_0 is far-detuned. Thus, relative to the phase of the $|0\rangle$ mode, a π phase shift is applied to the $|1\rangle \otimes |g_1\rangle$ component of the $|\text{photon}\rangle \otimes |\text{atom}\rangle$ quantum state, implementing the unitary transformation corresponding to a controlled-Z gate between the atom and the photon, $c\sigma_z = e^{i\pi|1\rangle\langle 1|\otimes|g_1\rangle\langle g_1|}$. After scattering, the photon passes back through the beam splitter and phase shifter and is returned to the storage ring. The joint state $|\Phi\rangle$ of the photon–atom system after a round trip through the scattering unit is

$$|\Phi\rangle = \left(Z_{\frac{\pi}{4}} B \otimes \mathbb{1}\right) c\sigma_z \left(BZ_{\frac{\pi}{4}} \otimes \mathbb{1}\right)(|\psi_{\text{in}}\rangle \otimes |+\rangle). \quad (1)$$

After the photon has returned to the storage ring, a rotation $R_x(-\theta) = \exp(i\sigma_x\theta/2)$ is applied to the atomic qubit. Finally, a projective measurement of the atomic state in the $\{|g_0\rangle, |g_1\rangle\}$ basis is performed, obtaining a bit $m \in \{0, 1\}$. As shown in Supplement 1 [56], this atomic measurement projects the state of the photonic qubit to

$$\begin{aligned} |\psi_{\text{out}}\rangle &= Z_{\frac{\pi}{4}}\sigma_z(-\sigma_y)^{m\oplus 1} R_y(\theta) Z_{\frac{\pi}{4}}|\psi_{\text{in}}\rangle \\ &= i^m Z_{\frac{5\pi}{4}} R_y(\theta + \pi(m \oplus 1))\, Z_{\frac{\pi}{4}}|\psi_{\text{in}}\rangle, \end{aligned} \quad (2)$$

where $R_y(\theta) = \exp(-i\sigma_y\theta/2)$, and $m \oplus 1$ denotes addition modulo 2. Thus, the measurement teleports the $R_x(\theta)$ rotation of the atom to the $R_y(\theta)$ or $R_y(\theta + \pi)$ rotation of the photon, depending on m. The full sequence of operations is shown in Fig. 2.

This teleportation scheme is an inversion of the paradigm of teleportation-based QC [57–59]: in both cases, the original data qubit is entangled with an ancilla using a $c\sigma_z$ operation, but instead of rotating and measuring the data qubit to teleport the modified state onto the ancilla, in our scheme, we rotate and measure the ancilla (the atom) to teleport a rotation onto the data qubit (the photon).

B. Constructing Arbitrary Single-Qubit Gates

We now show that the teleported gate operation of Eq. (2) is sufficient to construct arbitrary single-qubit gates. The purpose of the $Z_{\frac{\pi}{4}}$ operations performed by the phase shifter is to rotate the basis in which the $R_y(\theta)$ gate is applied. Two passes of a photon through the phase shifter corresponds to a rotation on the Bloch sphere [see Fig. 1(c)] about $\hat{z}$ by 90°; this change of basis causes a subsequent $R_y(\theta)$ to effectively rotate about $\hat{x}$. An additional two passes through the phase shifter rotates $\hat{x}$ to $-\hat{y}$, allowing $R_y(\theta)$ to act about $\hat{y}$ again. The goal here is to construct an operation that has the form $U = R_y(\theta_3)R_x(\theta_2)R_y(\theta_1)$, which is sufficient to implement any single-qubit gate up to an overall phase decomposed via Euler angles [57].

Consider a sequence of three teleported rotation gates (Eq. 2) about angles $\theta_1, \theta_2, \theta_3$ which yield measurement results m_1, m_2, m_3. As we build up the target operator U with these successive rotations, the outcomes m_1, m_2, m_3 can result in extraneous Pauli gates between rotations that effectively offset the target angles $\theta_1, \theta_2, \theta_3$ by π, as in the second line of Eq. (2). Intuitively, this is equivalent to constructing an arbitrary rotation in 3D space using only fixed 90° rotations about $\hat{z}$, together with variable rotations about $\hat{y}$, which may overshoot by π.

Borrowing a concept from measurement-based quantum computation [57,59,60], we apply rotations to the atomic qubit about *adaptive angles* of $\theta_2(m_1)$ and $\theta_3(m_2, m_1)$, each of which depends on the results of the preceding measurements. This allows us to propagate the Pauli errors from the middle of the gate to the front and consolidate them as a single error term. The sequence of three rotations performed in this adaptive basis thus implements the operation

$$U = \varepsilon(m_3, m_2, m_1) \times Z_{\frac{\pi}{4}} R_y(\theta_3(m_2, m_1))\, R_x(\theta_2(m_1))\, R_y(\theta_1) Z_{\frac{\pi}{4}}, \quad (3)$$

where the rotations are implicitly programmed to implement U in the basis rotated by $Z_{\frac{\pi}{4}}$ and where the error term $\varepsilon(m_3, m_2, m_1)$ is σ_x, σ_y, or σ_z up to a global phase. This error term ε can then either (i) be implicitly removed by programming a subsequent gate U' to instead implement $U'\varepsilon^{-1}$ or (ii) be explicitly removed by scattering the photon against the atom initialized in the noninteracting $|g_0\rangle$ state or in the fully interacting $|g_1\rangle$ state, applying σ_x or σ_z, respectively. The full derivation for this gate construction process is shown in much greater detail in Supplement 1 [56].

C. Two-Photon Gates

In addition to implementing single-qubit gates, a two-photon entangling gate is needed for universal computation. A controlled phase-flip gate $c\sigma_z$ between two photonic qubits j and k can be constructed through a sequence of three scattering interactions in a manner similar to the protocol described by Duan and Kimble [9]. However, the beam splitter and phase shifter, which are needed to implement the single-qubit gates in our scheme, allow us to apply

only operations of the form shown in Eq. (1) to the photon–atom system with each pass of a photon through the scattering unit. This prevents us from performing the exact protocol described in Ref. [9] despite the similarities of the proposed physical systems.

We can resolve this complication by modifying the protocol to terminate with a measurement on the atom. We denote the operation applied to the photon–atom state by a pass of photon j through the scattering unit interacting with the atom a as

$$\zeta^{ja} \equiv \left(Z_{\frac{\pi}{4}} B\right)^j c\sigma_z^{ja} \left(B Z_{\frac{\pi}{4}}\right)^j. \tag{4}$$

To implement $c\sigma_z^{jk}$ between photons j and k, we pass photon j through the scattering unit, then k, then j again, separated by $R_y(\pm\frac{\pi}{2})$ rotations applied to the atom [56]. This results in the state

$$\zeta^{ja} R_y^a(\pi/2)\zeta^{ka} R_y^a(-\pi/2)\zeta^{ja}\left(|\psi_{jk}\rangle \otimes |+\rangle\right), \tag{5}$$

where $|\psi_{jk}\rangle$ is the arbitrary state of photons j and k and where the atom is initialized to $|+\rangle$. After this scattering sequence, we measure the state of the atom, which projects the two-photon state to

$$\left(Z_{\frac{\pi}{4}} B \otimes Z_{\frac{\pi}{4}} B\right)\left(B Z_{(-1)^m \frac{\pi}{2}} B \otimes \mathbb{1}\right) \times c\sigma_z^{jk} \times \left(B Z_{\frac{\pi}{4}} \otimes B Z_{\frac{\pi}{4}}\right)|\psi_{jk}\rangle, \tag{6}$$

where the extraneous single qubit terms $BZ_{\frac{\pi}{4}}$, $Z_{\frac{\pi}{4}}B$, and $BZ_{(-1)^m\frac{\pi}{2}}B$ are artifacts of the photons passing through the beam splitter and phase shifter. These extra gates are not problematic: when constructing a circuit from single-qubit gates and $c\sigma_z$, they may be removed by programming previous and subsequent single-qubit gates to include inverse gates.

It is worth noting two alternative implementations of the photon–photon $c\sigma_z$ gate. First, using the SWAP operation implemented by Eq. (7), the states of one photonic qubit and the atom can be exchanged, and the second photon can directly interact with the state of the first, as discussed in Supplement 1 [56]. Second, the protocol demonstrated by Ref. [12] can be implemented on this system, reducing the amortized number of scattering passes per $c\sigma_z$.

Our proposed device can thus implement arbitrary single-qubit gates and a two-photon $c\sigma_z$ gate. This comprises a universal gate set [61], so the device can perform any quantum computation.

D. Arbitrary Circuit Compilation

To implement an arbitrary n-qubit operator $U \in \mathrm{U}(2^n)$, one could employ the three-step circuit compilation process outlined in Fig. 3. First, decompose U into a sequence of single-qubit gates and $c\sigma_z$ operations. This is a well-studied problem [62] and can be done using the same operator preparation routine described in our previous work [17], but with an additional $\mathcal{O}(n)$ speedup, as this scheme has all-to-all instead of nearest-neighbor connectivity between qubits. Second, represent each $c\sigma_z$ as in Eq. (6) and decompose each single-qubit gate via Euler angles into rotations that may be teleported onto the photonic qubits. Finally, use a classical control system to modify the adaptive rotations applied to the atomic qubit based on the measurement outcomes during operation and to explicitly correct for ε Pauli errors when necessary. A more detailed discussion of the compilation process and an example instruction sequence to implement a three-qubit quantum Fourier transform can be found in Supplement 1 [56].

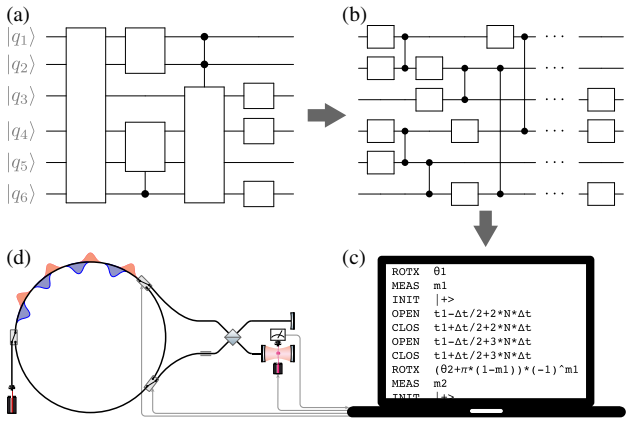

Fig. 3. Conceptual illustration of compiling a quantum circuit into an instruction sequence to be performed on the device. (a) Generic target quantum circuit. (b) Decomposition into an equivalent circuit of single-qubit and $c\sigma_z$ gates. (c) The circuit is further decomposed into a sequence of scattering interactions. This sequence can be assembled on a classical computer into an instruction set with six distinct primitives that correspond to physical actions. (d) The controllable elements of the quantum device are the optical switches, cavity laser, and atomic state readout.

E. Quantum State Readout

After applying the desired quantum operation using the circuit compilation routine outlined above, the state of the photonic qubits must be measured to obtain a classical result. This can be done without the need for single-photon detectors with their limited detection efficiencies by sequentially swapping the quantum states of each photonic qubit with that of the atom and repeatedly measuring the atomic state. To perform this SWAP operation, we scatter the desired photonic qubit j against the atom three times; between scattering operations, we apply the rotation $R_y(\pi/2)R_x(\pi)$ to the atomic qubit. Denoting this rotation as ρ^a and using ζ^{ja} as defined in Eq. (4), it is easily verified that

$$(BZ_{\frac{\pi}{4}})^j \zeta^{ja}\rho^a\zeta^{ja}\rho^a\zeta^{ja}(Z_{\frac{\pi}{4}}B)^j = e^{i\pi}\begin{pmatrix}1&0&0&0\\0&0&1&0\\0&1&0&0\\0&0&0&1\end{pmatrix}, \tag{7}$$

which is the SWAP operation up to a factor of -1. Here $(BZ_{\frac{\pi}{4}})^j$ and $(Z_{\frac{\pi}{4}}B)^j$ are the operations applied to photon j on the outgoing and return trip from the scattering unit, respectively [63]. Similar photon-atom and photon-ion swap operations have previously been experimentally demonstrated with high fidelity [64,65].

3. IMPERFECTION ANALYSIS

We now present a theoretical model to analyze the performance of our scheme in the presence of experimental imperfections. The main sources of error for our proposed scheme can be grouped into three classes: (i) deformation of the input pulse shape after scattering off the atom–cavity system, (ii) atomic spontaneous emission loss, and (iii) photon leakage due to attenuation and insertion loss while propagating through the storage ring and optical switches.

In our analysis, we assume the cavity mode frequency ω_c is exactly resonant with the atom $|g_1\rangle \leftrightarrow |e\rangle$ transition frequency

Ω_1, since the detuning can be calibrated to be zero in both free-space and nanophotonic systems [48]. Our design and simulations are agnostic to the carrier frequency [66]. We also assume that rotations of the atomic state using the cavity laser and measurement of the state can be done with fidelity $\mathcal{F} \approx 1$, as both processes have been demonstrated experimentally with infidelities significantly lower than the error sources listed above [47,67–71]. For all simulations here, we choose a photon pulse width of $\tau = 100/\kappa$ and time range (bin size) of $\Delta t = 500/\kappa$, and compute cooperativity with fixed $\gamma_s = \kappa/5$, where κ is the decay rate of the cavity into the waveguide, and γ_s is the atomic spontaneous emission rate. This choice of parameters was motivated by a sample of experimental cavity setups enumerated in Fig. 4 and results in a temporal bin size of order 100 ns for $\kappa/2\pi \sim 1$ GHz. Greater detail is given in Supplement 1 [56].

We use the analytical technique described by Shen and Fan [72,73] to exactly solve the single-photon transport problem of the coupled atom–cavity–waveguide system and obtain the output pulse $\phi_{\text{out}}(t)$ when the system is driven by an input pulse $\phi_{\text{in}}(t)$. This treatment captures the full quantum mechanical response of the system to a single-photon input Fock state for an arbitrary initialization of the atom without making the semiclassical assumption of a weak coherent input state.

Figure 4(a) shows the output pulse shapes for a single-photon Gaussian input pulse when the atom is initialized in states $|g_0\rangle$ or $|g_1\rangle$. For the $|g_0\rangle$ initialization, the response is identical to an empty cavity, since the $|g_0\rangle \leftrightarrow |e\rangle$ transition is far-detuned from the cavity resonant frequency. In this case, the output pulse is slightly delayed from the input pulse. For the $|g_1\rangle$ initialization, the photon is directly reflected from the front mirror of the cavity since the dressed cavity modes are well separated in the strong coupling limit from the input photon frequency by the vacuum Rabi splitting, so the delay is minimal. We denote the difference in the delays of the $|g_0\rangle$ and $|g_1\rangle$ scatterings as Δt_{01} (see inset). We compute the pulse shape fidelity $\mathcal{F}_{\text{shape}}$ as the overlap integral of the output pulse with the input pulse after both pulses have been normalized to have unit area, and the pulse shape infidelity is $1 - \mathcal{F}_{\text{shape}}$. This quantity describes only the mismatch of the shapes of the input and output pulses, not the mismatch of the pulse areas; the infidelity due to photon loss is computed as a separate quantity.

In Fig. 4(b), we plot the shape infidelity of various states as a function of the single-atom cavity cooperativity $C = 4g^2/\kappa\gamma_s$, where g is the atom–cavity coupling strength. The pulse shape infidelity from scattering off the $|g_1\rangle$ state decreases to negligible values as C increases, while the infidelity of $|g_0\rangle$ reaches an asymptote at 8×10^{-4} due to the delay of the output pulse by a time independent of C. The infidelity from scattering against $|+\rangle = (|g_0\rangle + |g_1\rangle)/\sqrt{2}$ thus reaches a value of 4×10^{-4}. Since the atom will usually be initialized to the $|+\rangle$ state during operation of the device, it is desirable to minimize the infidelity of this interaction. This can be done by equally distributing the delays between the $|g_0\rangle$ and $|g_1\rangle$ states by delaying the reference pulse by a time difference $\Delta t_{01}/2$, adding path length $c\,\Delta t_{01}/4$ to the top waveguide in Fig. 1(a). This results in a "delay corrected" infidelity of 2×10^{-4}, which is independent of both cavity cooperativity (for $C \gg 1$) and atomic state initialization.

In Fig. 4(b), we also plot the photon leakage probability for a scattering interaction. Atomic spontaneous emission noise from the excited $|e\rangle$ state into modes other than the cavity mode at a rate γ_s results in a partial loss of the photon, resulting in

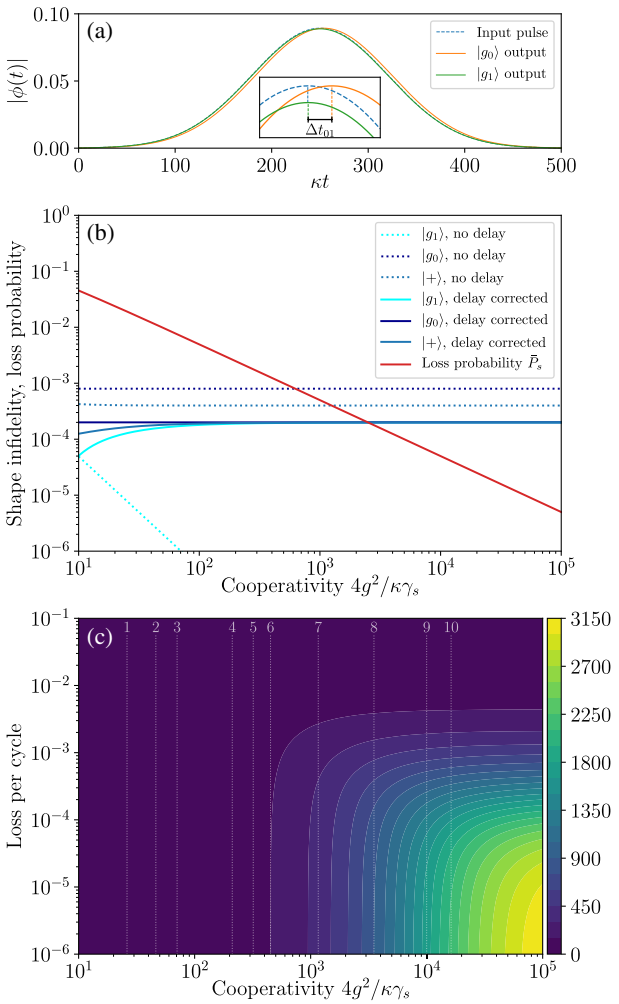

Fig. 4. (a) Output pulse shapes for $|g_0\rangle$ and $|g_1\rangle$ initialization when a cavity with cooperativity $C = 180$ is driven by a Gaussian input pulse. The inset highlights the behavior near maximum: the $|g_0\rangle$ output pulse is delayed, and the $|g_1\rangle$ output has reduced amplitude. (b) Shape infidelity and photon leakage probability as a function of cavity cooperativity. Solid blue lines show the pulse shape infidelity when the reference pulse is delayed by $\Delta t_{01}/2$. (c) Estimated single-qubit circuit depth achievable while maintaining >50% fidelity as a function of cavity cooperativity and photon attenuation per cycle, assuming one scattering interaction every cycle and no error correction. Dotted lines show various experimentally demonstrated cooperativity values in similar cavity systems. Lines 1–10 correspond respectively to Refs. [12,16,46,48–51,74,75], and [76].

an output pulse with total photon number $\int dt|\phi_{\text{out}}(t)|^2 < 1$. We calculate the probability P_s of spontaneous emission loss as $P_s = 1 - \frac{\int dt|\phi_{\text{out}}(t)|^2}{\int dt|\phi_{\text{in}}(t)|^2}$. Spontaneous emission noise applies only to the $|1\rangle \otimes |g_1\rangle$ component of the photon $\otimes$ atom state; since the atom will usually be initialized to the $|+\rangle$ state, if we average over the possible input photon states, we obtain an average leakage probability of $\bar{P}_s = P_s/4$. This average photon loss probability is plotted as the red line in Fig. 4(b) and ranges from about 5% to 0.0005% over the range of cooperativity values shown.

Finally, we account for loss due to attenuation in the optical storage ring and insertion loss from the switches as an average loss per cycle L. To estimate the maximum circuit depth D attainable with an overall fidelity $\mathcal{F}_{\text{target}}$, we compute a "bulk fidelity" per cycle accounting for shape infidelity, spontaneous emission loss,

and attenuation while propagating through the storage ring and optical switches. For simplicity, we assume the circuit operates on only a single photonic qubit and that the photon is scattered against the atom with every pass through the storage ring. The achievable circuit depth operating with success probability $\mathcal{F}_{\text{target}}$ is thus the maximum D satisfying $[\mathcal{F}_{\text{shape}} \times (1 - \bar{P}_s) \times (1 - L)]^D \geq \mathcal{F}_{\text{target}}$, which is plotted as a function of cavity cooperativity and propagation loss in Fig. 4(c) for $\mathcal{F}_{\text{target}} = 50\%$. Using optimistic but not unrealistic values for cooperativity [51,76,77] $C = 10^4$ and cycle loss $L = 10^{-4}$, we compute a bulk fidelity of $\mathcal{F} \approx 99.95\%$. This allows for an estimated depth of $D \approx 2000$ scattering operations while maintaining 50% success rate, and results in an error probability per gate (EPG) of $\sim 5 \times 10^{-4}$, below the estimated $\sim 10^{-3}$ EPG threshold for fault tolerance [78–81]. Additionally, photon loss, which is likely the main error mechanism, can be efficiently corrected up to a per-gate loss of $\sim 10^{-2}$ using concatenated codes [82].

4. DISCUSSION

In this work, we have shown how to use a single controllable quantum emitter to perform any quantum operation on a set of time-multiplexed photonic qubits. Related to but distinct from this paper are proposals for generating time- and frequency-multiplexed 2D cluster states using a single or pair of quantum emitters [83–86] or by using homodyne measurement of continuous-variable quantum systems [87], and experimental demonstrations using parametric nonlinearities [88,89]. Although 2D cluster states are a universal resource for measurement-based quantum computation [59], the schemes that prepare these states can apply only a single type of quantum operation to photonic qubits, and require single-photon detectors, with their associated limitations, for universality and state readout. In contrast, our scheme directly implements the quantum circuit model of QC, can deterministically construct any quantum gate, and can perform state readout without the need for photon detectors.

Our work also builds upon the well-known results of Ref. [9]. The physical setups are indeed similar: a cavity containing a controllable three-level atom that can mediate interactions between scattered photons. However, Ref. [9] showed how the atom–cavity system can apply a fixed $c\sigma_z$ operation to a pair of photonic qubits, while our work shows how a loop-based design incorporating the cavity can perform *any* quantum operation on any number of photonic qubits. Notably, the single-qubit gate teleportation mechanism described in Sections 2.A and 2.B and the photodetector-free circuit compilation and state readout routines described in Sections 2.D and 2.E are, to our knowledge, unique to this work.

The main practical advantage of our scheme is the experimental simplicity of the design. Compared to other photonic QC approaches, our scheme shows a pathway to implement scalable, deterministic, gate-based quantum computation with photonics. Also, our scheme does not require single-photon detectors, which are a limitation for photonic approaches due to their low detection efficiencies. Compared to other platforms for QC where qubits are individual physical structures, such as superconducting circuits and trapped ion systems, having only one controllable qubit provides a significant advantage to scalability: to add more qubits to our design requires just lengthening the fiber loop, while to add more qubits to a superconducting device requires adding complex individually addressable components.

However, our scheme is not without drawbacks: the design requires high cavity cooperativity and low fiber attenuation, which are challenging but feasible to implement [74], and it relies on optical switches with very low insertion losses, although recent advances in lithium niobate modulators [90] may soon allow for this. Additionally, although having only a single controllable qubit does greatly simplify the experimental setup, it prevents two-qubit and most single-qubit gates in a quantum circuit from being performed in parallel.

More broadly, if we generalize the photon storage mechanism for our proposed device and consider synthetic dimensions other than time multiplexing, we could potentially further improve the scalability of our design. Instead of using counterpropagating optical modes, one could encode each qubit in the polarization basis and combine with fiber or free-space storage loops, as in Refs. [91–93]. With suitable design of the atom–cavity interacting system, frequency [31,32] or angular momentum modes [41] could be also used as an alternative synthetic dimension, which could potentially mitigate the reliance of our design on low-loss optical switches, as demonstrated for heralded single-photon sources [94–97]. These concepts would naturally lend themselves to studying quantum many-body physics of interacting Hamiltonians in synthetic space [22], which is difficult to realize in purely photonic platforms without the strong single-photon nonlinearity of the atom that we employ here [98,99].

5. CONCLUSION

In this paper, we have presented a scheme for universal quantum computation using a single coherently controlled atom to indirectly manipulate a many-photon quantum state. We have shown that arbitrary single-qubit gates can be deterministically constructed from rotations applied to the atomic qubit and teleported onto photonic qubits via projective measurements. Using similar scattering processes, two-photon $c\sigma_z$ gates can be implemented, and readout of the photonic quantum state can be done using only atomic measurements with efficiencies far greater than that of state-of-the-art photon detectors. Our proposed scheme has high fidelity even in the presence of realistic experimental imperfections and offers significant advantages in required physical resources and experimental feasibility over many existing paradigms for photonic quantum computing.

Funding. U.S. Department of Defense (N00014-17-1-3030); U.S. Air Force Office of Scientific Research (FA9550-17-1-0002).

Disclosures. BB, AD, SF: Stanford Office of Technology Licensing (P).

Data availability. Calculations underlying the results in this paper are presented in Supplement 1. Simulation source code and computational notebooks may be obtained from the authors upon reasonable request.

Supplemental document. See Supplement 1 and Visualization 1 for supporting content.

REFERENCES AND NOTES

1. J. Wang, F. Sciarrino, A. Laing, and M. G. Thompson, "Integrated photonic quantum technologies," Nat. Photonics **14**, 273–284 (2020).
2. J. L. O'Brien, "Optical quantum computing," Science **318**, 1567–1570 (2007).

3. H.-S. Zhong, H. Wang, Y. H. Deng, M. C. Chen, L. C. Peng, Y. H. Luo, J. Qin, D. Wu, X. Ding, Y. Hu, and P. Hu, "Quantum computational advantage using photons," Science **370**, 1460–1463 (2020).
4. E. Knill, R. Laflamme, and G. J. Milburn, "A scheme for efficient quantum computation with linear optics," Nature **409**, 46–52 (2001).
5. P. Kok, B. Lagarde, A. Giuliani, G. A. Garcia, and L. Mercury, "Linear optical quantum computing with photonic qubits," Rev. Mod. Phys. **79**, 135–174 (2007).
6. Y. Li, P. C. Humphreys, G. J. Mendoza, and S. C. Benjamin, "Resource costs for fault-tolerant linear optical quantum computing," Phys. Rev. X **5**, 041007 (2015).
7. T. G. Tiecke, J. D. Thompson, N. P. de Leon, L. R. Liu, V. Vuletić, and M. D. Lukin, "Nanophotonic quantum phase switch with a single atom," Nature **508**, 241–244 (2014).
8. Q. A. Turchette, C. J. Hood, W. Lange, H. Mabuchi, and H. J. Kimble, "Measurement of conditional phase shifts for quantum logic," Phys. Rev. Lett. **75**, 4710–4713 (1995).
9. L. M. Duan and H. J. Kimble, "Scalable photonic quantum computation through cavity-assisted interactions," Phys. Rev. Lett. **92**, 127902 (2004).
10. A. Reiserer and G. Rempe, "Cavity-based quantum networks with single atoms and optical photons," Rev. Mod. Phys. **87**, 1379–1418 (2015).
11. H. Zheng, D. J. Gauthier, and H. U. Baranger, "Waveguide-QED-based photonic quantum computation," Phys. Rev. Lett. **111**, 090502 (2013).
12. B. Hacker, S. Welte, G. Rempe, and S. Ritter, "A photon–photon quantum gate based on a single atom in an optical resonator," Nature **536**, 193–196 (2016).
13. D. Tiarks, S. Schmidt-Eberle, T. Stolz, G. Rempe, and S. Dürr, "A photon–photon quantum gate based on Rydberg interactions," Nat. Phys. **15**, 124–126 (2019).
14. J. Volz, M. Scheucher, C. Junge, and A. Rauschenbeutel, "Nonlinear π phase shift for single fibre-guided photons interacting with a single resonator-enhanced atom," Nat. Photonics **8**, 965–970 (2014).
15. K. M. Beck, M. Hosseini, Y. Duan, and V. Vuletić, "Large conditional single-photon cross-phase modulation," Proc. Natl. Acad. Sci. USA **113**, 9740–9744 (2016).
16. I. Fushman, D. Englund, A. Faraon, N. Stoltz, P. Petroff, and J. Vučković, "Controlled phase shifts with a single quantum dot," Science **320**, 769–772 (2008).
17. B. Bartlett and S. Fan, "Universal programmable photonic architecture for quantum information processing," Phys. Rev. A **101**, 042319 (2020).
18. B. Machielse, S. Bogdanovic, S. Meesala, S. Gauthier, M. J. Burek, G. Joe, M. Chalupnik, Y. I. Sohn, J. Holzgrafe, R. E. Evans, and C. Chia, "Quantum interference of electromechanically stabilized emitters in nanophotonic devices," Phys. Rev. X **9**, 031022 (2019).
19. I. Aharonovich, D. Englund, and M. Toth, "Solid-state single-photon emitters," Nat. Photonics **10**, 631–641 (2016).
20. L. Yuan, Q. Lin, M. Xiao, and S. Fan, "Synthetic dimension in photonics," Optica **5**, 1396–1405 (2018).
21. O. Boada, A. Celi, J. I. Latorre, and M. Lewenstein, "Quantum simulation of an extra dimension," Phys. Rev. Lett. **108**, 133001 (2012).
22. T. Ozawa and H. M. Price, "Topological quantum matter in synthetic dimensions," Nat. Rev. Phys. **1**, 349–357 (2019).
23. E. Lustig, S. Weimann, Y. Plotnik, Y. Lumer, M. A. Bandres, A. Szameit, and M. Segev, "Photonic topological insulator in synthetic dimensions," Nature **567**, 356–360 (2019).
24. A. Regensburger, C. Bersch, M. A. Miri, G. Onishchukov, D. N. Christodoulides, and U. Peschel, "Parity–time synthetic photonic lattices," Nature **488**, 167–171 (2012).
25. M. Wimmer, H. M. Price, I. Carusotto, and U. Peschel, "Experimental measurement of the Berry curvature from anomalous transport," Nat. Phys. **13**, 545–550 (2017).
26. A. Marandi, Z. Wang, K. Takata, R. L. Byer, and Y. Yamamoto, "Network of time-multiplexed optical parametric oscillators as a coherent Ising machine," Nat. Photonics **8**, 937–942 (2014).
27. T. Inagaki, Y. Haribara, K. Igarashi, T. Sonobe, S. Tamate, T. Honjo, A. Marandi, P. L. McMahon, T. Umeki, K. Enbutsu, and O. Tadanaga, "A coherent Ising machine for 2000-node optimization problems," Science **354**, 603–606 (2016).
28. C. Leefmans, A. Dutt, J. Williams, L. Yuan, M. Parto, F. Nori, S. Fan, and A. Marandi, "Topological dissipation in a time-multiplexed photonic resonator network," arXiv:2104.05213 (2021).
29. B. Peng, S. Yan, D. Cheng, D. Yu, Z. Liu, V. V. Yakovlev, L. Yuan, and X. Chen, "Novel optical neural network architecture with the temporal synthetic dimension," arXiv:2101.08439 (2021).
30. P. L. McMahon, A. Marandi, Y. Haribara, R. Hamerly, C. Langrock, S. Tamate, T. Inagaki, H. Takesue, S. Utsunomiya, K. Aihara, and R. L. Byer, "A fully programmable 100-spin coherent Ising machine with all-to-all connections," Science **354**, 614–617 (2016).
31. L. Yuan, Y. Shi, and S. Fan, "Photonic gauge potential in a system with a synthetic frequency dimension," Opt. Lett. **41**, 741–744 (2016).
32. T. Ozawa, H. M. Price, N. Goldman, O. Zilberberg, and I. Carusotto, "Synthetic dimensions in integrated photonics: from optical isolation to four-dimensional quantum Hall physics," Phys. Rev. A **93**, 043827 (2016).
33. B. A. Bell, K. Wang, A. S. Solntsev, D. N. Neshev, A. A. Sukhorukov, and B. J. Eggleton, "Spectral photonic lattices with complex long-range coupling," Optica **4**, 1433–1436 (2017).
34. C. Reimer, S. Sciara, P. Roztocki, M. Islam, L. R. Cortés, Y. Zhang, B. Fischer, S. Loranger, R. Kashyap, A. Cino, and S. T. Chu, "High-dimensional one-way quantum processing implemented on d-level cluster states," Nat. Phys. **15**, 148 (2019).
35. Z. Yang, E. Lustig, G. Harari, Y. Plotnik, Y. Lumer, M. A. Bandres, and M. Segev, "Mode-locked topological insulator laser utilizing synthetic dimensions," Phys. Rev. X **10**, 011059 (2020).
36. K. Wang, B. A. Bell, A. S. Solntsev, D. N. Neshev, B. J. Eggleton, and A. A. Sukhorukov, "Multidimensional synthetic chiral-tube lattices via nonlinear frequency conversion," Light Sci. Appl. **9**, 132 (2020).
37. A. Celi, P. Massignan, J. Ruseckas, N. Goldman, I. B. Spielman, G. Juzeliūnas, and M. Lewenstein, "Synthetic gauge fields in synthetic dimensions," Phys. Rev. Lett. **112**, 043001 (2014).
38. M. Mancini, G. Pagano, G. Cappellini, L. Livi, M. Rider, J. Catani, C. Sias, P. Zoller, M. Inguscio, M. Dalmonte, and L. Fallani, "Observation of chiral edge states with neutral fermions in synthetic Hall ribbons," Science **349**, 1510–1513 (2015).
39. B. K. Stuhl, H.-I. Lu, L. M. Aycock, D. Genkina, and I. B. Spielman, "Visualizing edge states with an atomic Bose gas in the quantum Hall regime," Science **349**, 1514–1518 (2015).
40. A. Dutt, Q. Lin, L. Yuan, M. Minkov, M. Xiao, and S. Fan, "A single photonic cavity with two independent physical synthetic dimensions," Science **367**, 59–64 (2020).
41. X.-W. Luo, X. Zhou, C. F. Li, J. S. Xu, G. C. Guo, and Z. W. Zhou, "Quantum simulation of 2D topological physics in a 1D array of optical cavities," Nat. Commun. **6**, 7704 (2015).
42. L. Yuan, Q. Lin, A. Zhang, M. Xiao, X. Chen, and S. Fan, "Photonic gauge potential in one cavity with synthetic frequency and orbital angular momentum dimensions," Phys. Rev. Lett. **122**, 083903 (2019).
43. Y. Baum and G. Refael, "Setting boundaries with memory: generation of topological boundary states in Floquet-induced synthetic crystals," Phys. Rev. Lett. **120**, 106402 (2018).
44. I. Martin, G. Refael, and B. Halperin, "Topological frequency conversion in strongly driven quantum systems," Phys. Rev. X **7**, 041008 (2017).
45. The only components that act on the photonic qubits are the 50:50 beam splitter and $\pi/4$ phase shifter, which are fully static and serve only as a fixed change of basis of the photonic quantum state, and the optical switches, which actuate only between photon pulses in regions where the photon wave function is negligible.
46. Y. Colombe, T. Steinmetz, G. Dubois, F. Linke, D. Hunger, and J. Reichel, "Strong atom–field coupling for Bose–Einstein condensates in an optical cavity on a chip," Nature **450**, 272–276 (2007).
47. R. Gehr, J. Volz, G. Dubois, T. Steinmetz, Y. Colombe, B. L. Lev, R. Long, J. Esteve, and J. Reichel, "Cavity-based single atom preparation and high-fidelity hyperfine state readout," Phys. Rev. Lett. **104**, 203602 (2010).
48. P. Samutpraphoot, T. Đorđević, P. L. Ocola, H. Bernien, C. Senko, V. Vuletić, and M. D. Lukin, "Strong coupling of two individually controlled atoms via a nanophotonic cavity," Phys. Rev. Lett. **124**, 063602 (2020).
49. J. McKeever, A. Boca, A. D. Boozer, J. R. Buck, and H. J. Kimble, "Experimental realization of a one-atom laser in the regime of strong coupling," Nature **425**, 268–271 (2003).
50. J. P. Covey, A. Sipahigil, S. Szoke, N. Sinclair, M. Endres, and O. Painter, "Telecom-band quantum optics with ytterbium atoms and silicon nanophotonics," Phys. Rev. Appl. **11**, 034044 (2019).
51. D. Chang, J. Douglas, A. González-Tudela, C.-L. Hung, and H. Kimble, "Colloquium: quantum matter built from nanoscopic lattices of atoms and photons," Rev. Mod. Phys. **90**, 031002 (2018).

52. C. Monroe, "Quantum information processing with atoms and cavities," Nature **416**, 238–246 (2002).
53. J. McKeever, A. Boca, A. D. Boozer, R. Miller, J. R. Buck, A. Kuzmich, and H. J. Kimble, "Deterministic generation of single photons from one atom trapped in a cavity," Science **303**, 1992–1994 (2004).
54. L. M. Duan, A. Kuzmich, and H. J. Kimble, "Cavity QED and quantum-information processing with "hot" trapped atoms," Phys. Rev. A **67**, 032305 (2003).
55. To avoid time bin conflicts, the optical switches are asymmetrically placed in the storage ring. If the top switch is placed k time bins (a distance $k\,c\Delta t$) from the horizontal midpoint of the ring, then, as shown in Fig. 1(a), the bottom switch is placed at a distance $(k+1/2)c\Delta t$ from the midpoint, and the waveguide it connects to is $c\Delta t/2$ shorter than its counterpart. This ensures that when the bottom switch is set to the open state, directing a counterclockwise pulse into the bottom waveguide, the nearest clockwise pulse is $c\Delta t/2$ distance away.
56. See Supplement 1 for more detailed derivations of the gate teleportation mechanism, construction of arbitrary single-qubit rotations, construction of a two-photon $c\sigma_z$ gate, construction of a photon–atom SWAP gate, an example of a compiled instruction sequence for a quantum Fourier transform, and a more detailed discussion of the imperfection analysis described in this work.
57. R. Jozsa, "An introduction to measurement based quantum computation," arXiv:0508124 (2005).
58. D. Gottesman and I. L. Chuang, "Quantum teleportation is a universal computational primitive," arXiv:9908010 (1999).
59. M. A. Nielsen, "Cluster-state quantum computation," Rep. Math. Phys. **57**, 147–161 (2006).
60. R. Raussendorf and H. J. Briegel, "A one-way quantum computer," Phys. Rev. Lett. **86**, 5188–5191 (2001).
61. A. Barenco, C. H. Bennett, R. Cleve, D. P. DiVincenzo, N. Margolus, P. Shor, T. Sleator, J. A. Smolin, and H. Weinfurter, "Elementary gates for quantum computation," Phys. Rev. A **52**, 3457–3467 (1995).
62. M. Mottonen and J. J. Vartiainen, "Decompositions of general quantum gates," arXiv:0504100 (2005).
63. This construction of the SWAP gate starts with the photon in the middle of the scattering unit. If one starts with the photon in the storage ring, the state SWAPed to the atom is actually $BZ_{\frac{\pi}{4}}|\psi_j\rangle$. As before, this can be resolved by including $(BZ_{\frac{\pi}{4}})^{-1}$ in preceding single-qubit gates. Alternately, the atomic state can be directly manipulated after the SWAP gate is applied and before measurement to remove the extraneous $BZ_{\frac{\pi}{4}}$.
64. O. Bechler, A. Borne, S. Rosenblum, G. Guendelman, O. E. Mor, M. Netser, T. Ohana, Z. Aqua, N. Drucker, R. Finkelstein, Y. Lovsky, R. Bruch, D. Gurovich, D. Shafir, and B. Dayan, "A passive photon–atom qubit swap operation," Nature Phys. **14**, 996–1000 (2018).
65. A. Borne, T. E. Northup, R. Blatt, and B. Dayan, "Efficient ion-photon qubit SWAP gate in realistic ion cavity-QED systems without strong coupling," Opt. Express **28**, 11822–11839 (2020).
66. In practice, the carrier frequency is chosen according to the transition frequency of the atomic qubit. If, for example, the atomic qubit is assumed to be a ^{87}Rb atom, the carrier frequency will be chosen to be $\omega_c \approx 3.8\times10^{14}$ Hz [12].
67. C. D. Bruzewicz, J. Chiaverini, R. McConnell, and J. M. Sage, "Trapped-ion quantum computing: progress and challenges," Appl. Phys. Rev. **6**, 021314 (2019).
68. A. Bermudez, X. Xu, R. Nigmatullin, J. O'Gorman, V. Negnevitsky, P. Schindler, T. Monz, U. G. Poschinger, C. Hempel, J. Home, and F. Schmidt-Kaler, "Assessing the progress of trapped-ion processors towards fault-tolerant quantum computation," Phys. Rev. X **7**, 041061 (2017).
69. A. H. Myerson, D. J. Szwer, S. C. Webster, D. T. C. Allcock, M. J. Curtis, G. Imreh, J. A. Sherman, D. N. Stacey, A. M. Steane, and D. M. Lucas, "High-fidelity readout of trapped-ion qubits," Phys. Rev. Lett. **100**, 200502 (2008).
70. T. P. Harty, D. T. C. Allcock, C. J. Ballance, L. Guidoni, H. A. Janacek, N. M. Linke, D. N. Stacey, and D. M. Lucas, "High-fidelity preparation, gates, memory, and readout of a trapped-ion quantum bit," Phys. Rev. Lett. **113**, 220501 (2014).
71. A. H. Burrell, D. J. Szwer, S. C. Webster, and D. M. Lucas, "Scalable simultaneous multiqubit readout with 99.99% single-shot fidelity," Phys. Rev. A **81**, 040302 (2010).
72. J. T. Shen and S. Fan, "Theory of single-photon transport in a single-mode waveguide. I. Coupling to a cavity containing a two-level atom," Phys. Rev. A **79**, 059904 (2009).
73. J. T. Shen and S. Fan, "Theory of single-photon transport in a single-mode waveguide. II. Coupling to a whispering-gallery resonator containing a two-level atom," Phys. Rev. A **79**, 023838 (2009).
74. R. Miller, T. E. Northup, K. M. Birnbaum, A. D. B. A. Boca, A. D. Boozer, and H. J. Kimble, "Trapped atoms in cavity QED: coupling quantized light and matter," J. Phys. B **38**, S551–S565 (2005).
75. X. Li, M. Bamba, Q. Zhang, S. Fallahi, G. C. Gardner, W. Gao, M. Lou, K. Yoshioka, M. J. Manfra, and J. Kono, "Vacuum Bloch–Siegert shift in Landau polaritons with ultra-high cooperativity," Nat. Photonics **12**, 324–329 (2018).
76. A. Suleymanzade, A. Anferov, M. Stone, R. K. Naik, A. Oriani, J. Simon, and D. Schuster, "A tunable high-Q millimeter wave cavity for hybrid circuit and cavity QED experiments," Appl. Phys. Lett. **116**, 104001 (2020).
77. T.-H. Chang, B. M. Fields, M. E. Kim, and C.-L. Hung, "Microring resonators on a suspended membrane circuit for atom-light interactions," Optica **6**, 1203–1210 (2019).
78. M. A. Nielsen and I. L. Chuang, *Quantum Computation and Quantum Information*, 10th anniversary ed. (Cambridge University, 2010).
79. D. Gottesman, "Stabilizer codes and quantum error correction," Ph.D. thesis (California Institute of Technology, 1997).
80. J. Preskill, "Fault-tolerant quantum computation," arXiv:9712048 (1997).
81. E. Knill, "Quantum computing with realistically noisy devices," Nature **434**, 39–44 (2005).
82. E. Knill, R. Laflamme, and G. Milburn, "Thresholds for linear optics quantum computation," arXiv:0006120 (2000).
83. H. Pichler, S. Choi, P. Zoller, and M. D. Lukin, "Universal photonic quantum computation via time-delayed feedback," Proc. Natl. Acad. Sci. USA **114**, 11362–11367 (2017).
84. S. E. Economou, N. Lindner, and T. Rudolph, "Optically generated 2-dimensional photonic cluster state from coupled quantum dots," Phys. Rev. Lett. **105**, 093601 (2010).
85. Y. Zhan and S. Sun, "Deterministic generation of loss-tolerant photonic cluster states with a single quantum emitter," Phys. Rev. Lett. **125**, 223601 (2020).
86. M. Victora, F. Kaneda, F. Bergmann, J. J. Wong, A. Graf, and P. Kwiat, "Time-multiplexed methods for optical quantum information processing," in *Quantum Photonics: Pioneering Advances and Emerging Applications*, R. W. Boyd, S. G. Lukishova, and V. N. Zadkov, eds. (Springer International Publishing, 2019), Vol. **217**, pp. 179–206.
87. S. Takeda and A. Furusawa, "Toward large-scale fault-tolerant universal photonic quantum computing," APL Photon. **4**, 060902 (2019).
88. W. Asavanant, Y. Shiozawa, S. Yokoyama, B. Charoensombutamon, H. Emura, R. N. Alexander, S. Takeda, J. I. Yoshikawa, N. C. Menicucci, H. Yonezawa, and A. Furusawa, "Generation of time-domain-multiplexed two-dimensional cluster state," Science **366**, 373–376 (2019).
89. M. V. Larsen, X. Guo, C. R. Breum, J. S. Neergaard-Nielsen, and U. L. Andersen, "Deterministic generation of a two-dimensional cluster state," Science **366**, 369–372 (2019).
90. C. Wang, M. Zhang, B. Stern, M. Lipson, and M. Lončar, "Nanophotonic lithium niobate electro-optic modulators," Opt. Express **26**, 1547–1555 (2018).
91. K. R. Motes, A. Gilchrist, J. P. Dowling, and P. P. Rohde, "Scalable boson sampling with time-bin encoding using a loop-based architecture," Phys. Rev. Lett. **113**, 120501 (2014).
92. P. P. Rohde, "Simple scheme for universal linear-optics quantum computing with constant experimental complexity using fiber loops," Phys. Rev. A **91**, 012306 (2015).
93. T. B. Pittman and J. D. Franson, "Cyclical quantum memory for photonic qubits," Phys. Rev. A **66**, 062302 (2002).
94. C. Joshi, A. Farsi, S. Clemmen, S. Ramelow, and A. L. Gaeta, "Frequency multiplexing for quasi-deterministic heralded single-photon sources," Nat. Commun. **9**, 847 (2018).
95. F. Kaneda and P. G. Kwiat, "High-efficiency single-photon generation via large-scale active time multiplexing," Sci. Adv. **5**, eaaw8586 (2019).
96. C. Joshi, A. Farsi, A. Dutt, B. Y. Kim, X. Ji, Y. Zhao, A. M. Bishop, M. Lipson, and A. L. Gaeta, "Frequency-domain quantum interference with correlated photons from an integrated microresonator," Phys. Rev. Lett. **124**, 143601 (2020).

97. S. Massar and S. Clemmen, "Resource efficient single photon source based on active frequency multiplexing," Opt. Lett. **46**, 2832–2835 (2021).
98. L. Yuan, A. Dutt, M. Qin, S. Fan, and X. Chen, "Creating locally interacting Hamiltonians in the synthetic frequency dimension for photons," Photon. Res. **8**, B8–B14 (2020).
99. T. Ozawa and I. Carusotto, "Synthetic dimensions with magnetic fields and local interactions in photonic lattices," Phys. Rev. Lett. **118**, 013601 (2017).